

## Supplementary Information for:

# Shaping Crystals with Light: Crystal-to-Crystal Isomerization and Photomechanical Effect in Fluorinated Azobenzenes

Oleksandr S. Bushuyev, Anna Tomberg, Tomislav Friščić\* and Christopher J. Barrett\*

Department of Chemistry and FRQNT Centre for Self-Assembled Chemical Structures, McGill University, 801 Sherbrooke St. W., H3A 0B8, Montreal, Canada

## Table of Contents

<b>1. Experimental</b>	S2
1.1 Materials	S2
1.2 Syntheses	S2
1.3 UV-Vis spectra	S4
1.4 Photomechanical motion measurements	S6
<b>2. Videos and images of photomechanical crystal motion</b>	S6
<b>3. Single crystal X-ray diffraction data measurements and crystallographic summary</b>	S7
3.1 Description of crystal structures	S8
3.2 Summary of indexing the crystal of <i>cis</i> -1 after irradiation	S10
<b>4. Powder X-ray diffraction data</b>	S11
<b>5. Theoretical calculations</b>	S12
<b>6. References</b>	S16

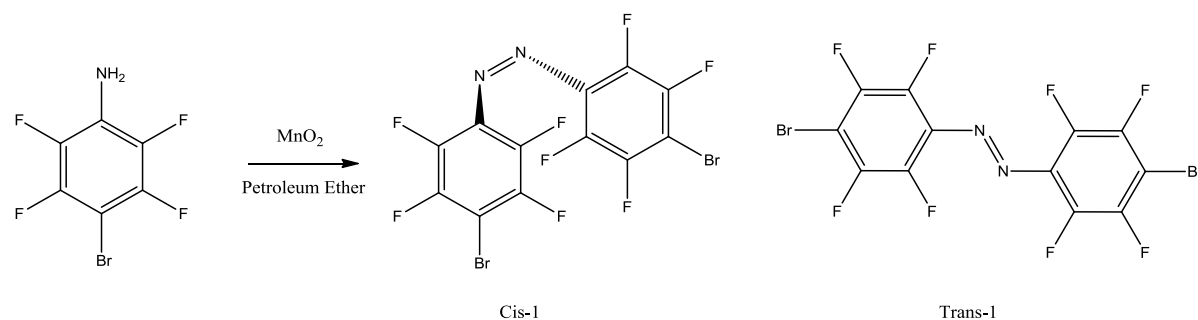
## 1. Experimental

### 1.1 Materials

4-Bromo-2,3,5,6-tetrafluoroaniline, 2,3,5,6-tetrafluoroaniline and mercury oxide were obtained from Sigma Aldrich and used without purification. Activated manganese dioxide was obtained in house from potassium permanganate and manganese sulfate utilizing a published procedure.

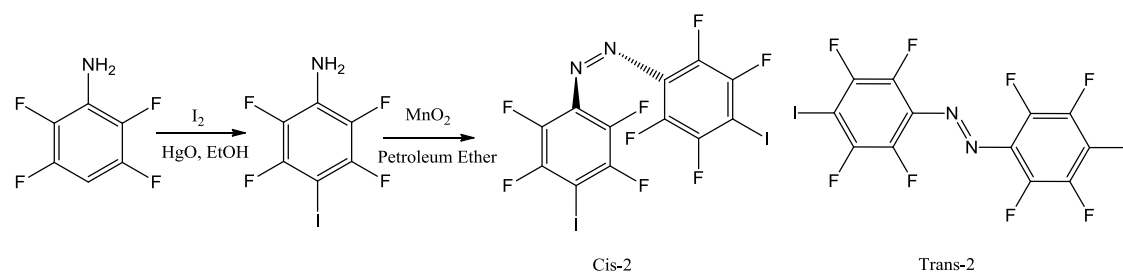
### 1.2 Syntheses

#### 4,4'-dibromooctafluoroazobenzene (**1**)



600 mg of 4-Bromo-2,3,5,6-tetrafluoroaniline was mixed with 8.2 g of activated manganese dioxide in 100 ml of petroleum ether. After 6 days of stirring at room temperature the slurry was filtered, washed until clear washings with petroleum ether and then with dichloromethane (DCM). All fractions were combined, and solvent was removed on rotary evaporator. Product was purified on CombiFlash automated silica column, using 95% hexane 5% ethyl acetate gradient solvent system. Yield 182 mg of cis (30.5%) and 80 mg trans (13.4%).\*

#### 4-iodo-2,3,5,6-tetrafluoroaniline



400 mg of yellow (1.84 mmol) HgO was added to a solution of 450 mg (2.45 mmol) of 2,3,5,6-tetrafluoroaniline in 20 ml of ethanol. Mixture was stirred for 30 minutes, and then 620 mg (2.44 mmol) of I<sub>2</sub> was added. Mixture was stirred overnight and then filtered over celite. Solvent was removed on rotary evaporator, then product redissolved in ca. 40 ml of DCM and washed several times with saturated Na<sub>2</sub>S<sub>2</sub>O<sub>3</sub> solution and dried over MgSO<sub>4</sub>. Product was purified by sublimation yielding long needles 605 mg, (85%).<sup>1</sup>H-NMR: broad signal at 4.1 ppm.

#### 4,4'-diiodooctafluoroazobenzene(2)

600 mg of previously synthesized 4-iodo-2,3,5,6-tetrafluoroaniline was mixed with 8.0 g of activated manganese dioxide in 100 ml of petroleum ether. After 3 days of stirring at room temperature the slurry was filtered, washed until clear washing with petroleum ether and then with dichloromethane (DCM). All fractions were combined, and solvent was removed on rotary evaporator. Product was purified on CombiFlash automated silica column, using 95% hexane 5% ethyl acetate gradient solvent system. Yield 120 mg of *cis*-**2** (20%) and 70 mg *trans*-**2** (11.7%).\*

Chemical identities of the prepared compounds were confirmed by single crystal X-ray diffraction, powder X-ray diffraction (e.g. see Figure S7) and absence of proton signals in <sup>1</sup>H-NMR spectrum.

\*Yield of *trans*-form can be enhanced by refluxing the mixture. However, upon refluxing the amount of isolated *cis*-isomer drops significantly.

### 1.3 Uv-Vis spectra

UV-Vis studies of *cis-trans* isomerization were performed using a Cary 300 Bio UV-Vis spectrometer. For the thermal relaxation study absorption was monitored at 320 nm for **1** and 330 nm for **2**. *K*-values and  $t_{1/2}$  were obtained for **1** in hexanes, THF, and DCM; for **2** in hexanes and are summarized in Table S1. Example UV-Vis spectra are given in Figure S1, compositions of the photostationary state and thermal *cis-trans* relaxation are given in Figure 2S. Molar extinction coefficients ( $\epsilon$ ) were determined to be 12200 L·mol<sup>-1</sup>·cm<sup>-1</sup> for *cis-1* at  $\lambda$ =420 nm and 8000 L·mol<sup>-1</sup>·cm<sup>-1</sup> at  $\lambda$ =460 nm for *trans-1*.

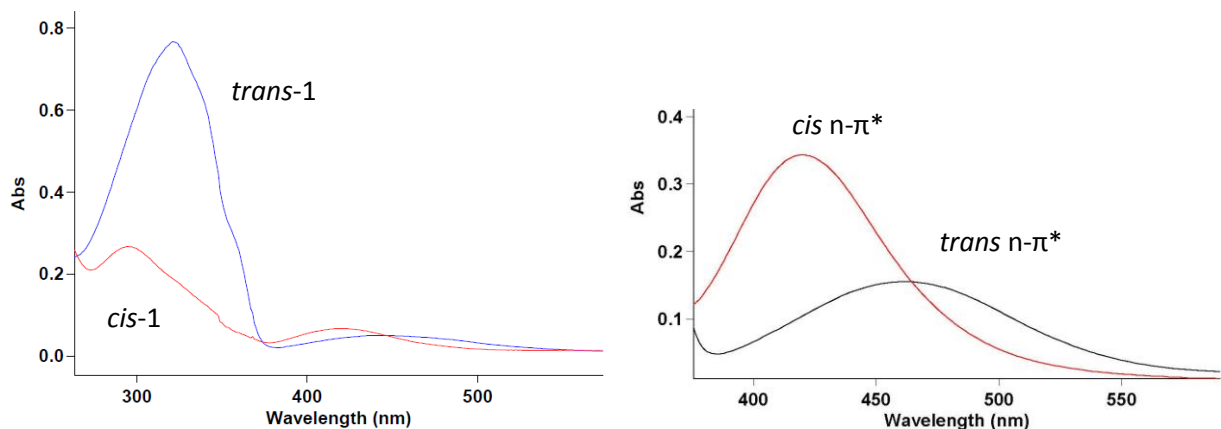


**Figure S1.**(left) UV-Vis profile of *cis-1* (red) and *trans-1* (blue) in hexanes; (right)  $n-\pi^*$  transitions for *cis-1* (red) and *trans-1* (black)

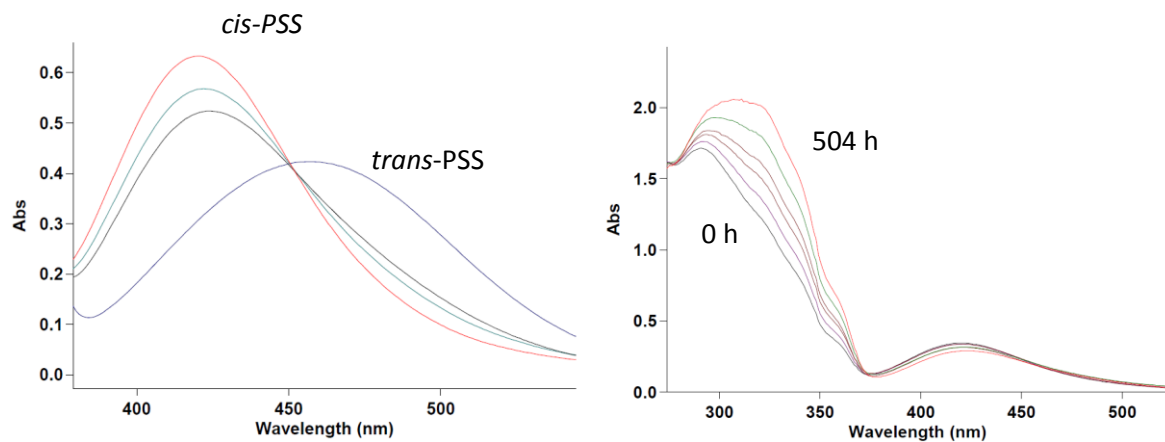


**Figure S2.** (left) Photostationary states (PSS) for **1**. Red - near 100% of *cis-1* achieved by 10mW (532 nm) laser irradiation for 60 minutes. Blue – PSS containing 90% *trans-1* achieved by 1mW (405 nm) laser irradiation for 140 minutes. (right) UV-Vis trace of *cis-1* relaxation in hexanes over 3 weeks of experiment at 0, 72, 166, 242, 362 and 504 hours.

**Table S1** Half-lives of *cis*-isomers and reaction constants for **1** and **2**.

compound (solvent)	<i>cis</i> -1 (hexanes)	<i>cis</i> -1 (THF)	<i>cis</i> -1 (DCM)	<i>cis</i> -2 (hexanes)
$K, (s^{-1})$	$2.75 \times 10^{-7}$	$1.93 \times 10^{-7}$	$1.34 \times 10^{-7}$	$2.23 \times 10^{-7}$
$t_{1/2}, \text{ days}$	29	42	60	36

The lack of back (*trans*→*cis*) isomerization in the solid in the current system may be explained by nearly coincident absorption/transmission maxima for both *cis*- and *trans*-isomers as shown in Figure S3:

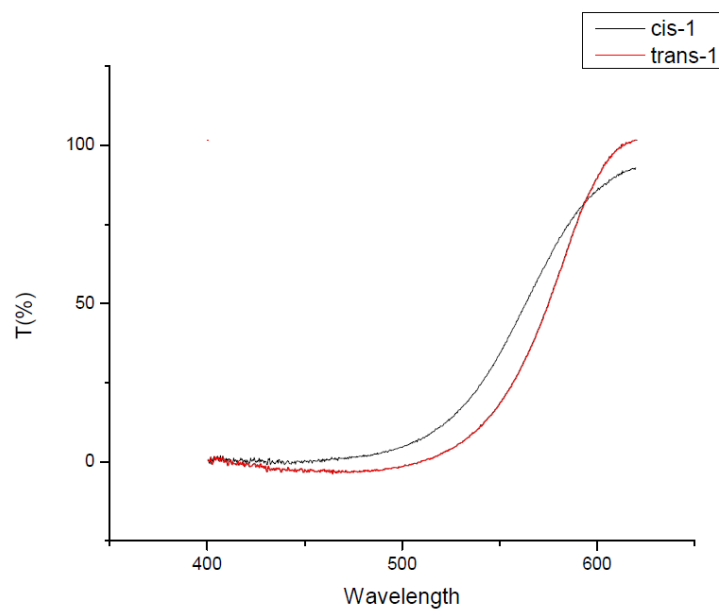


**Figure S3.** Solid-state spectra of *cis*- and *trans*- isomers of **1**.

## 1.4 Photomechanical motion measurements

Needle-like crystals of 1 and 2 of approximately 10-20  $\mu\text{m}$  thickness were selected and subjected to irradiation on the tip of the Mitegen<sup>®</sup> 75  $\mu\text{m}$  aperture micromounts with the nominal tip thickness of 10  $\mu\text{m}$ . Irradiation was achieved by linearly polarized variable power Ar<sup>+</sup>-ion laser at 457 nm wavelength. Beam power used for experiments was 1-5 mW, with beam diameter slightly less than 1  $\text{mm}^2$ . Photomechanical motion was recorded by the Infinity-1 CMOS microscopy camera fitted with a zoom lens.

## 2. Videos and images of photomechanical crystal motion

All videos are recorded and presented in real time.

Video S1. Bending of the *cis*-1 crystal when subjected to 457 nm blue laser light at power equal to 5 mW. The crystal curls, reaching tip deflection of nearly 180° and remains stationary after the end of irradiation.

Video S2. Upon the irradiation of the crystal from Video S1 from the opposite side, the crystal first straightens and then curls in a backward direction. After two opposite faces were irradiated in such a fashion the crystal becomes completely inactive in the laser light.

Video S3. S-shaping by irradiating a section of the crystal on one face, then rotating the mount, raising the crystal and irradiating the section on the opposite face.

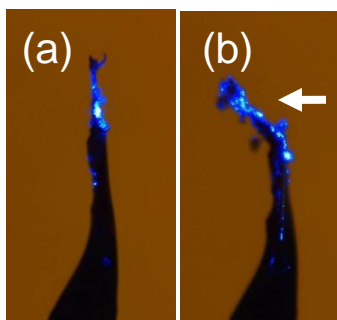


**Figure S4.** Permanent photomechanical modification of *cis*-2 crystal aggregate by irradiation: (a) crystal before irradiation and (b) after irradiation. Direction of irradiation is indicated by the white arrow.

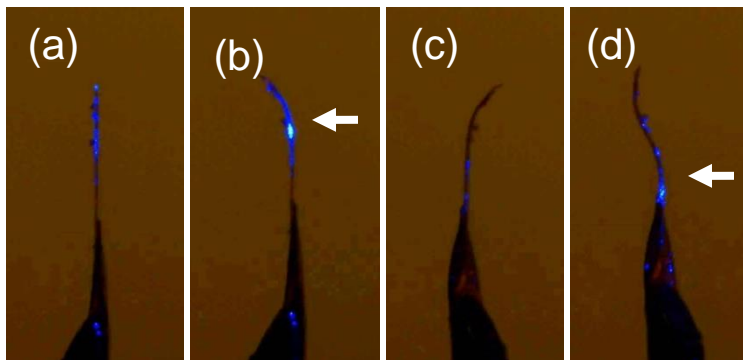


**Figure S5.** Permanent S-shape photomechanical modification of *cis*-1 crystal by irradiation: (a) crystal before irradiation; (b) crystal after irradiation; (c) crystal after rotation by 180° around its long axis and (d) crystal after second turn of irradiation. Direction of irradiation is indicated by the white arrow.

### 3. Single crystal X-ray diffraction measurements and crystallographic summary

X-ray diffraction data was obtained on Bruker D8 single-crystal X-ray diffractometer equipped with a MoK $\alpha$  X-ray source and a graphite monochromator. Multi-scan absorption correction (SADABS) was applied. Structures were solved by direct methods and refined using SHELX-97 software.<sup>1</sup> Data summary is presented in Tables S1 and S2.

**Table S2.** General and crystallographic data for compounds **1** and **2**.

compound	<i>cis</i> - <b>1</b>	<i>cis</i> - <b>1a</b>	<i>trans</i> - <b>1</b>	<i>cis</i> - <b>1</b> , irradiated	<i>cis</i> - <b>2</b>	<i>trans</i> - <b>2</b>
formula	C <sub>12</sub> N <sub>2</sub> F <sub>8</sub> Br <sub>2</sub>	C <sub>12</sub> N <sub>2</sub> F <sub>8</sub> Br <sub>2</sub>	C <sub>12</sub> N <sub>2</sub> F <sub>8</sub> Br <sub>2</sub>	C <sub>12</sub> N <sub>2</sub> F <sub>8</sub> Br <sub>2</sub>	C <sub>12</sub> N <sub>2</sub> F <sub>8</sub> Br <sub>2</sub>	C <sub>12</sub> N <sub>2</sub> F <sub>8</sub> Br <sub>2</sub>
$\rho_{\text{calc}}$ (g/cm <sup>3</sup> )	2.368	2.373	2.470	2.333	2.668	2.625
crystal system	Monoclinic	Monoclinic	Monoclinic	Monoclinic	Monoclinic	Monoclinic
<i>T</i> (K)	150	100	100	293	100	100
space group	<i>C</i> 2/ <i>c</i>	<i>C</i> 2/ <i>c</i>	<i>P</i> 2 <sub>1</sub> / <i>c</i>	<i>P</i> 2 <sub>1</sub> / <i>c</i>	<i>C</i> 2/ <i>c</i>	<i>P</i> 2 <sub>1</sub> / <i>n</i>
unitcell parameters	<i>a</i> =23.402(2) Å <i>b</i> =5.3155(5) Å <i>c</i> =11.676(1) Å $\beta$ =110.802(1)°	<i>a</i> =13.707(3) Å <i>b</i> =5.597(1) Å <i>c</i> =18.138(3) Å $\beta$ =103.254°	<i>a</i> =10.250(2) Å <i>b</i> =7.636(1) Å <i>c</i> =8.742(1) Å $\beta$ =108.010(2)°	<i>a</i> =8.89(2) Å <i>b</i> =7.79(2) Å <i>c</i> =10.57(2) Å $\beta$ =109.55(2)°	<i>a</i> =24.454(2) Å <i>b</i> =5.3242(5) Å <i>c</i> =11.826(1) Å $\beta$ =109.769(1)°	<i>a</i> =10.324(1) Å <i>b</i> =5.9680(6) Å <i>c</i> =24.112(2) Å $\beta$ =100.176(1)°
unitcell volume (Å <sup>3</sup> )	1357.7(2)	1354.5(4)	650.7(2)	690(2)	1448.9(2)	1462.3(2)
<i>Z</i>	4	4	2	2	4	4
resolution (°)	25.00	26.73	26.01	17.27	26.73	25.00
completeness (%)	99.7	99.6	99.9	40.7	99.8	99.7
collected/independent reflections	7084/1441	5029/1433	6538/1289	984/172	7508/1538	8044/3303
data/parameters/restraints	1441/109/0	1433/109/0	1289/109/0	172/36/	1538/109/0	3303/398/307
<i>S</i>	1.60	1.063	1.073	1.287	1.047	1.035
<i>R</i> <sub>1</sub> [for <i>I</i> ≥ 4σ( <i>I</i> )]	0.0200	0.0183	0.0175	0.1169	0.0219	0.0270
<i>R</i> <sub>1</sub> , <i>wR</i> <sub>2</sub> (for all data)	0.0216, 0.0520	0.0210, 0.0455	0.0191, 0.0462	0.1293, 0.3035	0.0266, 0.0563	0.0367, 0.0601
largest diff. peak, hole (e Å <sup>-3</sup> )	0.443, -0.484	0.345, -0.343	0.556, -0.315	0.872, -1.031	0.674, -0.440	0.362, -0.724

### 3.1 Description of crystal structures

For all the crystal structures, see the CIF files also provided in the Supplementary Information. The *trans*-isomers of **1** and **2** in the solid state assemble into different motifs: *trans*-**1** forms  $\pi$ -stacks composed of identically oriented molecules, while *trans*-**2**, probably due to a larger radius of the iodine atom adopts a herringbone structure with two distinct orientations for the azo molecules. In both structures the fluorinated phenyl rings are coplanar, despite possible repulsive interactions between ortho-fluorine atoms. Both **1** and **2** in the *trans*-form exhibit pedaling motion observed as a disorder of the azo group.

Crystal structures of *cis*-**1** and *cis*-**2** contain alternately-oriented stacks of V-shaped molecules parallel to the crystallographic *b*-axis. A distinct difference in intramolecular angles between the phenyl planes can be seen when comparing to the parent azobenzene molecule. The angle between the phenyl rings opens up from  $64^\circ$  in the parent azobenzene to  $81^\circ$  and  $74^\circ$  in *cis*-**1** and *cis*-**1a**, respectively, and  $82^\circ$  in *cis*-**2** (Figures S6 and S7). Such a difference is significant as the effective volume change upon azo isomerization is likely to be determined by the relative positioning of the phenyl rings and distance between the termini of the azo molecules. In most previous investigations, an angle of  $64^\circ$  between phenyl planes is quoted even for molecules significantly different than parent azobenzene.

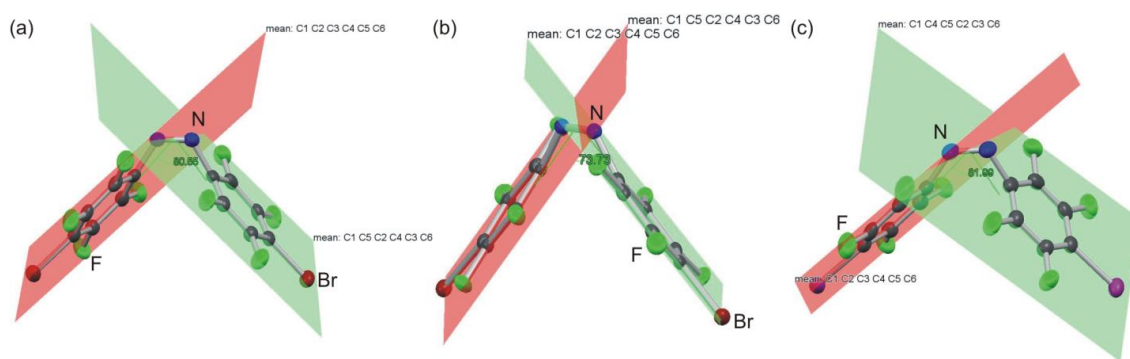


**Figure S6.** Molecular geometries for: (a) *cis*-**1**; (b) *cis*-**1a** and (c) *cis*-**2** in corresponding single crystal structures. The depicted planes (red and green) correspond to best planes drawn through the benzene rings of the 4-bromo- and 4-iodotetrafluorophenyl groups. Figures drawn using Mercury CSD.

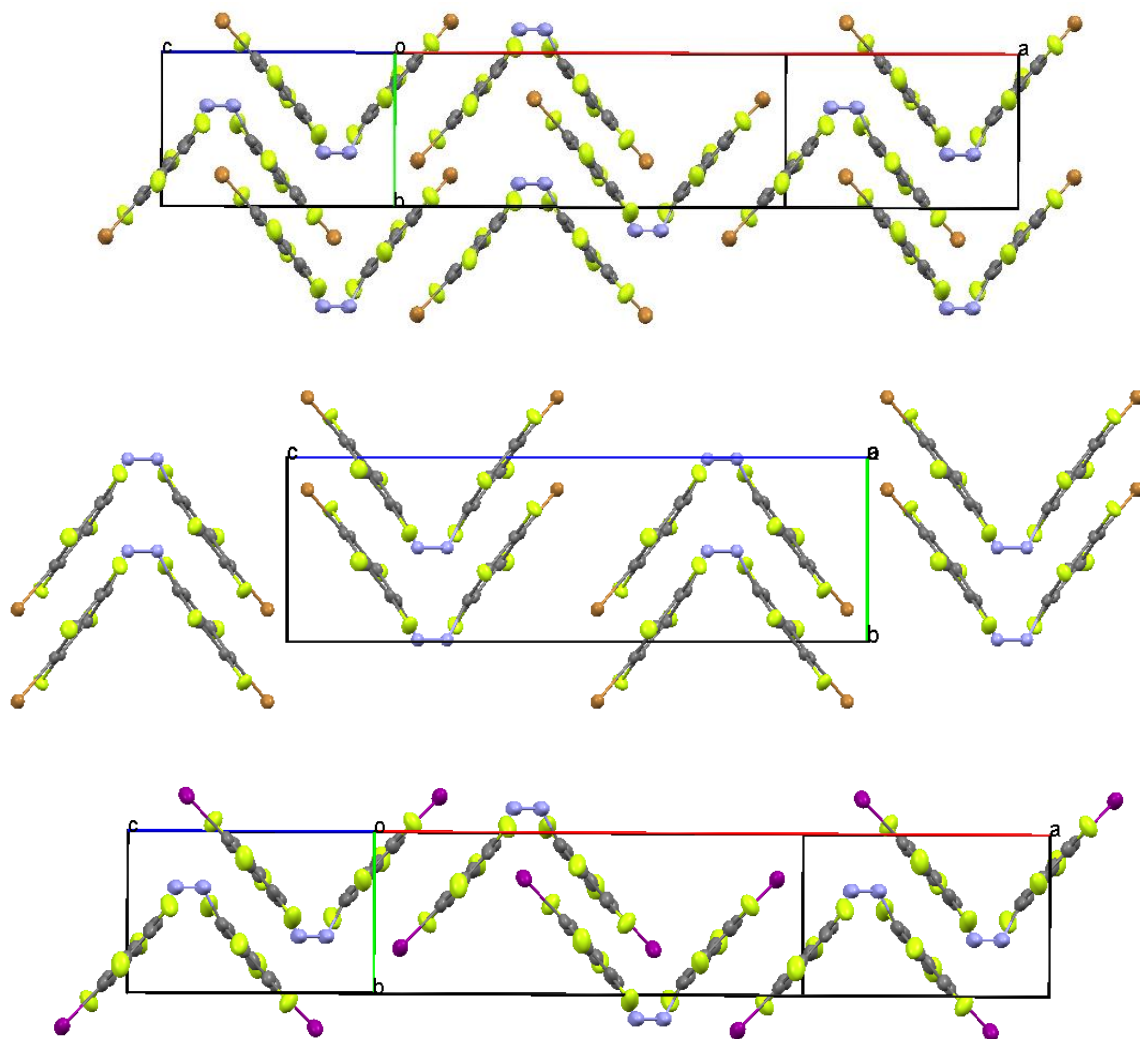


**Figure S7.** Crystal packing of: (top) *cis-1* viewed perpendicular to the crystallographic *ab*-plane; (middle) *cis-1a* viewed down crystallographic *a*-axis and (bottom) *cis-2* viewed perpendicular to the crystallographic *ab*-plane. Note the isostructural nature of *cis-1* (top) and *cis-2* (bottom). Figures were drawn using Mercury CSD.

### 3.2 Summary of indexing the crystal of *cis-1* after irradiation

Majority of the reflections (903 out of 1125) could be fitted to five major domains<sup>2</sup>, described below:

Domain 1: 446 reflections out of 1125

Domain 2: rotated by 178.8 degrees about reciprocal 1.000; -0.182; -0.515; 382 reflections, (204 exclusively)

Domain 3: rotated by 7.0 degrees about reciprocal 1.000; -0.240; -0.178; 286 reflections (129 exclusively)

Domain 4: rotated by 103.1 degrees about reciprocal 0.024; 0.009; 1.000; 318 reflections (69 exclusively)

Domain 5: rotated by 174.1 degrees about reciprocal 1.000; -0.184; -0.508; 337 reflections (55 exclusively)

The remaining 222 reflections are all fitted if a total of 16 domains are considered. All 16 domains exhibit the same unitcell (identical to the second decimal) resembling that of *trans-1*:  $a=8.894\text{ \AA}$ ,  $b=7.790\text{ \AA}$ ,  $c=10.572\text{ \AA}$ ,  $\beta=109.55^\circ$ .

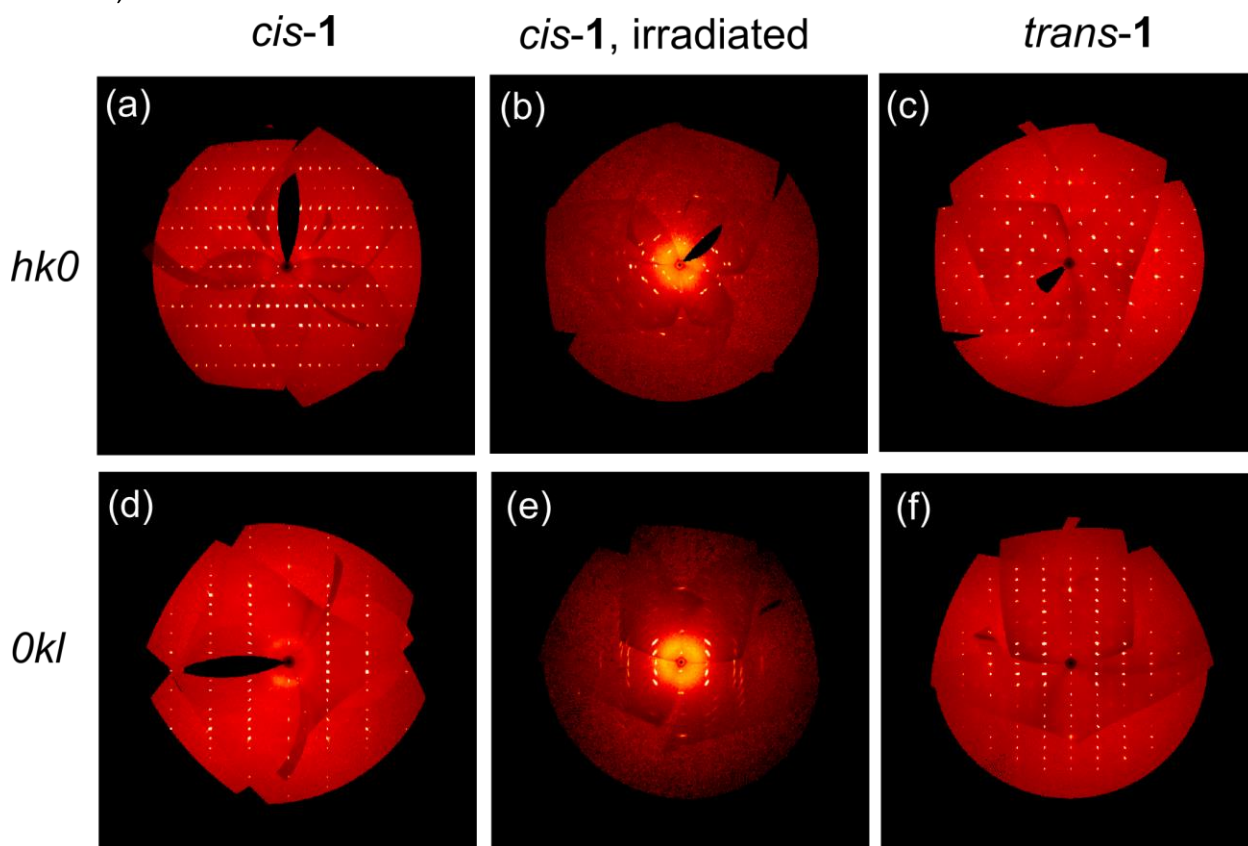


**Figure S8.** Composite diffraction images for the *hk0* diffracting plane of: (a) *cis-1*; (b) *cis-1* irradiated at 457 nm for 4 hours; (c) *trans-1* and the *0kl* diffracting plane of: (d) *cis-1*; (e) *cis-1* irradiated at 457 nm for 4 hours; (f) *trans-1*. The d-spacings measured for images (b) and (e) clearly matched those in images (c) and (f), respectively.

#### 4. Powder X-ray diffraction data

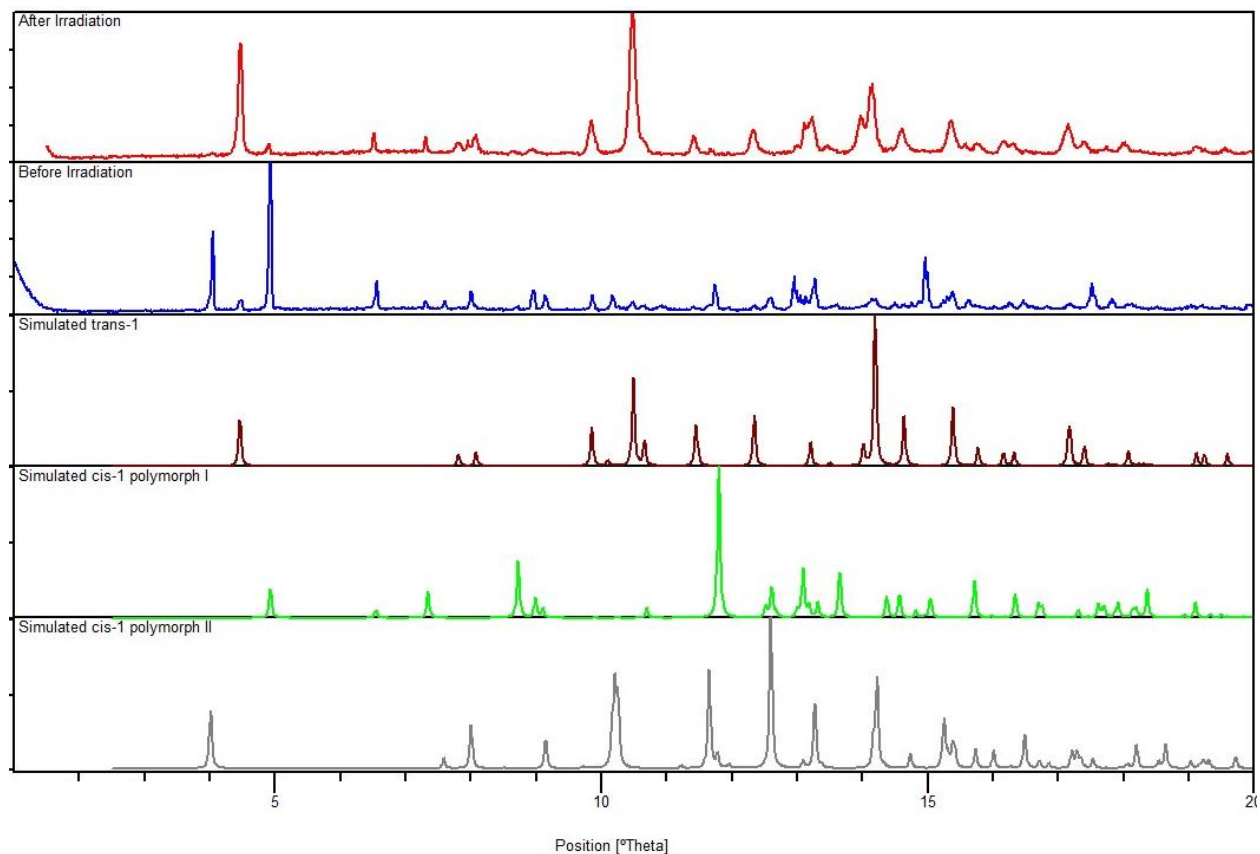


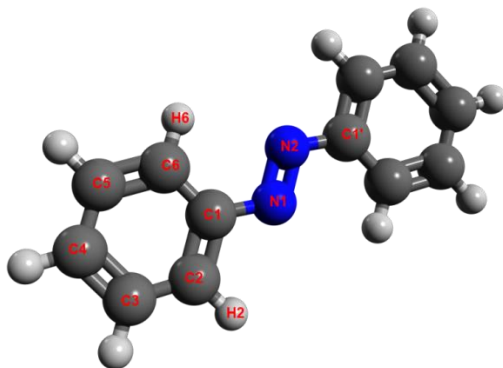
**Figure S9.** Powder X-ray diffraction patterns for the bulk irradiation experiment. From top to bottom: sample of *cis-1* after irradiation; sample of *cis-1* before irradiation; simulated pattern of *trans-1*; simulated patterns for the two polymorphs of *cis-1*.

## 5. Theoretical calculations

All calculations were performed using the Gaussian package<sup>3</sup> and Avogadro<sup>4</sup> was used as visualization software. The basis set a level of theory were chosen based on the results of a validation study for azobenzene *trans*- and *cis*-conformations. As shown in Table S3, the best compromise between accuracy and time was a DFT hybrid method B3LYP yielding the right geometry. Also, Pople's 6-31G(d) basis set was found to be suitable for azobenzene parent molecules as well as for **1**, while **2** required a bigger basis set to suite iodine, and DGDZVP was used.

The accuracy of the theoretical model was based on the best structural geometry obtained compared to experimental results for *cis* and *trans* azobenzene molecules. In order to effectively cover the various possibilities, a variety of theoretical model types were used: a semi-empirical PM6 method, two *ab initio* methods (HF, MP2), and a density functional method (B3LYP). Basis sets used in combination with these models had different levels of polarizability and different number of diffuse functions so that the impact of the size of basis set on the accuracy of results could be monitored.

As shown in Table S4, the MP2/6-31+G(d) combination displays the smallest average percent error, making it the most accurate. However, this computation is the only one that predicted a non-planar geometry for *trans*-azobenzene (torsion angle of 17.5°), which makes its geometry optimization unacceptable. The next best combination was found to be MP2/6-311+G(d,p), yet computational time significantly exceeded the desired threshold of 2 hours. For these reasons, the third best combination, B3LYP/6-31G(d), was selected for geometry optimization of subsequent *trans*-azobenzene derivatives. Notably, polarization and the increased number of diffuse functions in the orbital approximation of basis sets yielded equivalent or worse results than the normal 6-31G(d) basis set. Other, least successful combinations were attempted but are not shown in Table S3.

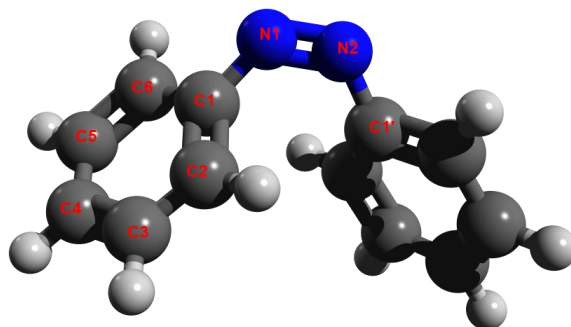


**Figure S10.** Molecular model of *trans*-azobenzene (atoms are labeled as in Table S3).

**Table S3.** Geometry optimization of *trans*-azobenzene.

Bond lengths (Å)						
	Atom 1	Atom 2	MP2/6-31+G(d)	MP2/6-311+G(d,p)	B3LYP/6-31G(d)	Experimental <sup>5</sup>
	N (1)	N (2)	1.279	1.271	1.261	1.243
	C (1)	N (1)	1.423	1.423	1.419	1.433
	C (1)	C (2)	1.402	1.403	1.401	1.384
	C (1)	C (6)	1.405	1.407	1.406	1.385
	C (2)	H (2)	1.088	1.087	1.086	1.102
	C (6)	H (6)	1.087	1.085	1.084	1.102
Bond angles (degrees)						
Atom 1	Atom 2	Atom 3	MP2/6-31+G(d)	MP2/6-311+G(d,p)	B3LYP/6-31G(d)	
C (1)	N (1)	N (2)	113.4	113.9	114.8	113.6
C (2)	C (1)	N (1)	115.3	114.9	115.3	115.5
C (6)	C (1)	N (1)	124.0	124.7	124.8	
C (2)	C (1)	C (6)	120.7	120.4	119.9	120.3
C (1)	C (6)	C (5)	119.1	119.2	119.6	119.6
C (1)	C (2)	C (3)	119.7	120.0	120.2	119.6
C (1)	C (6)	H (6)	119.5	119.4	118.8	
C (1)	C (2)	H (2)	118.7	118.4	118.2	
Torsion angles:		D(C <sub>2</sub> ,C <sub>1</sub> ,N <sub>1</sub> ,N <sub>2</sub> )	162.5	180.0	180.0	180.0
		D(C <sub>1</sub> ',N <sub>2</sub> ,N <sub>1</sub> ,C <sub>1</sub> )	177.6	180.0	180.0	
%error (average on 4 references) <sup>6</sup> :			1.02	1.04	1.07	

Using the optimal B3LYP/6-31G(d) combination, the geometry of *cis*-azobenzene was also computed and the bond lengths, bond angles and the C-N=N-C torsion angle were compared with experimental values taken from the literature. The results were collected in Table S4, where the atoms are labeled as in Figure S11.

**Figure S11.** Molecular model for *cis*-azobenzene, atoms are labeled as in Table S4.

**Table S4.** Optimized geometry of *cis*-azobenzene using B3LYP/6-31G(d).

Bond lengths (Å)						
	Atom 1	Atom 2	B3LYP/6-31G(d)	Experimental <sup>[7]</sup>	%error	
	N (1)	N (2)	1.243	1.253	0.8	
	C (1)	N (1)	1.436	1.448	0.9	
	C (1)	C (2)	1.401	1.385	1.2	
	C (2)	C (3)	1.391	1.377	1.0	
	C (3)	C (4)	1.394	1.389	0.4	
	C (4)	C (5)	1.395	1.374	1.5	
	C (5)	C (6)	1.390	1.378	0.9	
	C (6)	C (1)	1.398	1.401	0.2	
Bond angles (degrees)						
	Atom 1	Atom 2	Atom 3			
	C (1)	N (1)	N (2)	124.2	121.9	1.8
	C (2)	C (1)	N (1)	122.9	122.5	0.3
	C (1)	C (2)	C (3)	120.1	120.8	0.6
	C (2)	C (3)	C (4)	120.5	119.0	1.2
	C (3)	C (4)	C (5)	119.8	121.7	1.6
	C (4)	C (5)	C (6)	120.1	118.7	1.2
	C (5)	C (6)	C (1)	120.0	119.8	0.2
	C (2)	C (1)	C (6)	119.9	120.0	0.1
	Torsion angle:		D(6,7,5,14)	51.0	53.0	3.7
				Total %error:	1.0	

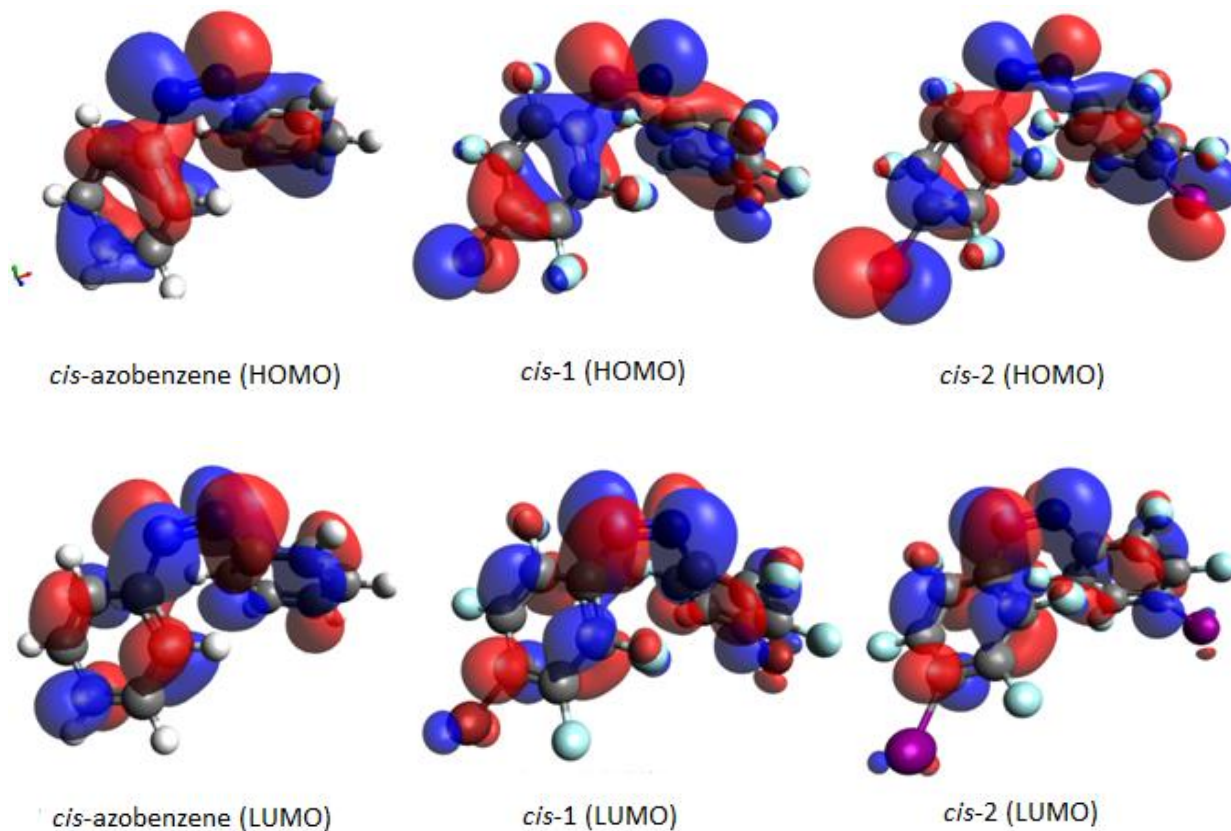
The values obtained were in agreement with literature displaying a similar percent error as the one for *trans*-azobenzene. Especially, the torsion angle of the C=N=N-C bond was found to be 51°, which was shown to be the correct geometry of *cis*-azobenzene in several studies.<sup>8</sup> It was concluded that B3LYP/6-31G(d) is the optimal combination for computations on *trans*-azobenzene and *cis*-azobenzene molecules and their derivatives.

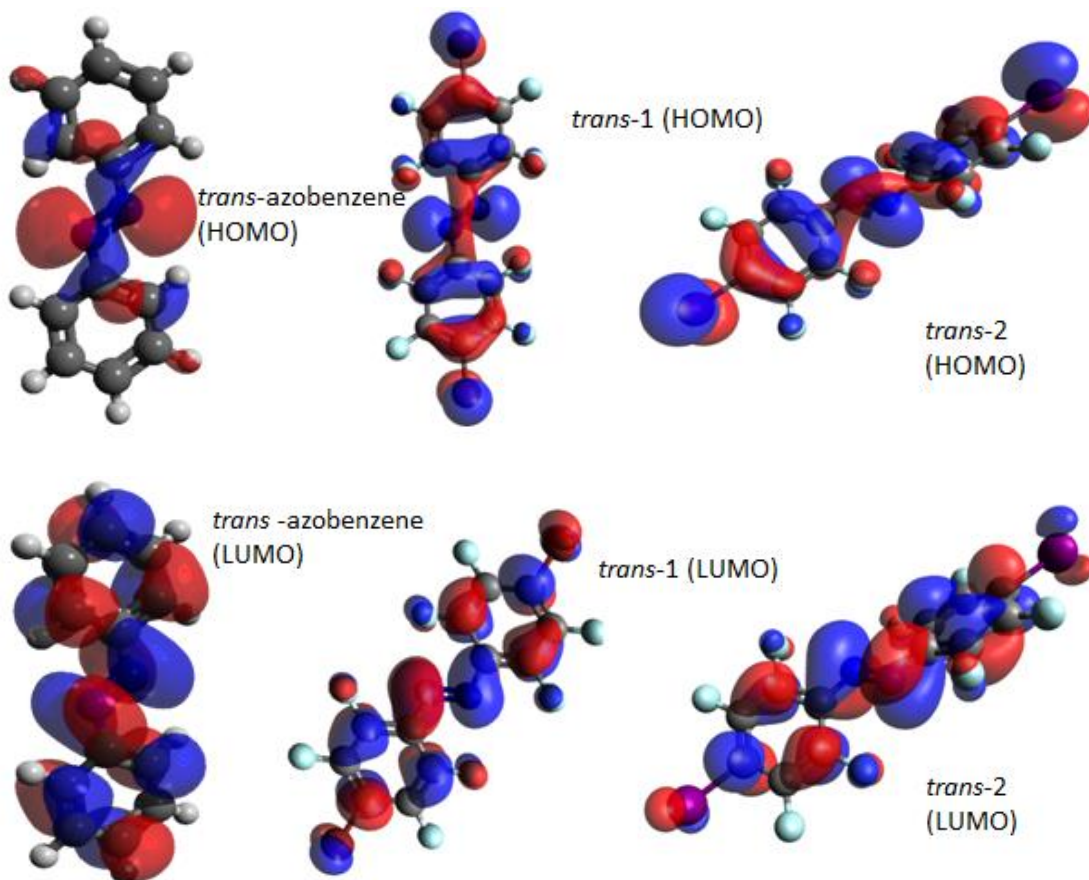
To ensure that the results obtained for **1** and **2** were realistic, their geometry was compared to the parent azobenzene molecule. For all structures, first a geometry optimization was performed, followed by a vibrational analysis, where no imaginary frequencies were found, meaning that the geometries obtained correspond to the ground state structures in gas phase. In order to compare the isomers of each compound, the difference in their single point energies were computed. The result obtained for azobenzene corresponds to the values seen in literature.<sup>9</sup> Energy differences between *cis*- and *trans*-isomers of **1** and **2** are very similar, approximately half the value for azobenzene. All these results are summarized in Table S5.

**Table S5.** Results of DFT calculations.

Structure		1		2		Parent azobenzene	
Method		B3LYP/6-31G(d)		B3LYP/DGDZVP		B3LYP/6-31G(d)	
	Units	cis	trans	cis	trans	cis	trans
$\Delta$ SP(trans-cis)	kcal/mol	8.84		8.88		15.26	
Dipole moment	Debye	1.74	0.06	2.52	0.10	3.21	0.00
$\Delta$ LUMO-HOMO	eV	3.78	3.55	3.66	3.40	3.76	3.95
CN=NC Torsion angle	°	10.58	178.18	9.97	177.07	9.36	179.97
N=NCC Torsion angle	°	56.37	23.21	57.57	23.21	51.03	0.01

Finally the molecular orbitals of all isomers were computed. The corresponding figures of HOMO and LUMO orbitals are shown below:





## 6. References

- [1] Sheldrick, G. M. *Acta Cryst.*, **2008**, A64, 112.
- [2] Sheldrick, G. M. (2004). *CELL\_NOW*. University of Göttingen, Germany.
- [3] Gaussian, Inc., Gaussian 09, Revision B-0.1.
- [4] Hanwell, M.D., et al., *Avogadro: an advanced semantic chemical editor, visualization, and analysis platform*. *J. Cheminform.*, **2012**, 4, 17.
- [5] Chen, P.C.; Chieh, Y.C. *J. Mol. Struct.*, **2003**, 624, 191.
- [6] (a) Fliegl H. et al. *J. Am. Chem. Soc.* **2003**, 125, 9821 ; (b) Biswas N.; Umapathy S. *J. Phys. Chem. A*, **1997**, 101, 5555.
- [7] Armstrong, D. R. et al. *J. Phys. Chem.* **1995**, 99, 17825.
- [8] (a) Kurita, N. et al. *Chem. Phys. Lett.* **2002**, 360, 349; (b) Sauer, P.; Allen, R.E. *Chem. Phys. Lett.* **2008**, 450, 192.
- [9] Crecca, C.R.; Roitberg, A.E. *J. Phys. Chem. A*, **2006**, 110, 8188.